COBEM 2023 27TH INTERNATIONAL CONGRESS OF MECHANICAL ENGENEERING

ABCM Brazilian Society of Mechanical Sciences and Engineering
27th ABCM International Congress of Mechanical Engineering
December 04-08, 2023, Florianópolis-SC, Brazil

DESIGN AND KINEMATIC ANALYSIS OF A FLAPPING WING MECHANISM FOR OPTIMIZED BIO-INSPIRED UAV

Maurício Menegatti Andrade[1]
Mariana Finamor Frota Saldanha de Freitas[2]
Augusto Salomão Bornschlegell[3]
Rodrigo Borges Santos[4]
Federal University of Grande Dourados (UFGD), Faculty of Engineering, Department of Mechanical Engineering, Dourados, MS, Brazil
[1]mauricio.menean@gmail.com; [2]marianafffsaldanha@yahoo.com.br; [3]augustosalomao@ufgd.edu.br; [4]rodrigobsantos@ufgd.edu.br

Douglas D. Bueno
São Paulo State University (UNESP), School of Engineering, Department of Mathematics, Ilha Solteira, SP, Brazil
douglas.bueno@unesp.br

Abstract. *Biomimetics is a science that seeks to emulate natural systems and phenomena in order to solve human problems and innovate in engineering. Given that context, biomimetic mechanisms are those whose function is inspired by some natural parallel. Similarly, Flapping Wing Air Vehicles, or FWAVs, are biomimetic models designed to fly. However, in contrast to the already common and known models of aircraft, like airplanes, helicopters and drones, FWAVs mimic with greater fidelity their biological counterparts' characteristics. These mechanisms aim to replicate the capacity of insects and birds to lift themselves and move through air with agility, using only their wings as propulsion. In that way, FWAVs dismiss the need for conventional aerial propulsion, such as propellers and jet engines. Taking advantage of their wings' lift, these models can be a much more versatile aircraft design, allowing swift, agile and smooth movement, alongside implementations at a significantly smaller scale. In tandem with their potential, FWAVs present a great engineering challenge, mainly on the context of energy efficiency, weight reduction and wear of the mechanical parts. With those needs in mind, this article presents the mathematical modelling of an Ornithopter (a biomimetic mechanism inspired by a birds' wing) using two mirrored four-bar mechanisms and a simple single crank and double rocker system. Such mechanism, despite its simplicity, has the disadvantage of asynchrony between its wings. Therefore, our focus on this work is optimizing the design parameters to minimize asynchrony and achieve a general performance improvement, following guidelines from existing literature. The use of complex numbers and Euler notation, sometimes combined with vector notation, enabled further simplifications to the conventional mathematical model of the four-bar linkage. That way, a more intuitive and concise implementation was possible using Python.*

Keywords: *Flapping-Wing-Air-Vehicles, Mechanism, Optimization, Biomimetics*

1. INTRODUCTION

When considering contemporary aerial vehicles, two common designs come to mind. The majority of commercial flying aircraft can be classified as either rotor-wing vehicles, encompassing helicopters and drones, or fixed-wing aircraft, such as airplanes. Both categories are already well established and developed. However, contemplating modern advancements and designs in the area, a distinct class emerges: flapping-wing air vehicles.

Flapping-wing air vehicles (FWAVs) are biomimetic devices which mimic the flying mechanism and ability of some biological organisms. Particularly, ornithopters are inspired by the structure and function of a bird's wings. FWAVs pose a great advancement for aviation: they dismiss the need for conventional aerial propulsion, enabling compact aircraft design, achieving smaller sizes and swift movement. Mastering the control over an ornithopter's wings would pave the way for aircraft with a never-before seen versatility and proficiency in flight.

Some functional prototypes were already developed and are worthy of mention. The SmartBird, by Festo's Bionic Learning Network, presented by Send *et al.* (2012), is a fully functional ornithopter capable of take off, flight and landing. The vertical motion of it's wings is driven by an electric motor and controlled by two rotating wheels that compose it's mechanism. The wings are also capable of twisting, which is essential to the maneuverability and aerodynamics of the FWAV.

Mimicking a peregrine falcon, the RoBird is also a great example of an ornithopter. It is a commercial FWAV developed by Aerium Analytics and used for wildlife management at airfield and agricultural applications. In addition to it's flying ability, the RoBird's similarity to a peregrine falcon is it's main tool to avert wildlife at particular areas. We can see then that an ornithopter has a vast range of applications and has the potential to revolutionize some activities.

While an ornithopter functioning involves high speed movement and a relatively complex mechanism, it also needs to have low energy use and reduced weight. That way, it is critical to optimize the mechanism's performance and mechanical simplicity. However, as will be noted in the next section, procuring simpler mechanisms leads us to issues with synchrony, which can impair the ornithopter aerodynamic performance. For that reason, the focus of this work is to optimize the parameters of a minimal wing design in order to reach maximum synchrony.

The mechanism developed in this paper will be similar to the one presented by Shi *et al.* (2022). And to meaningfully analyze it's performance and synchrony, criteria presented in existing literature will be checked for the resulting mechanism. Arenas (2016) observes some geometrical and angular parameters necessary for best function of the device. We will also refer to YANG and Esakki (2021) for experimental data on the ornitopther's stability and performance as consequence of it's relevant angular ranges.

2. THE WING STRUCTURE

The wing structure of avian species can be subdivided, regarding mechanics, as inner and outer wing (seen on Fig. (1)). A single-part wing following a simple arch trajectory would create as much lift going down as it does going up, being unable to sustain flight. But the combined movement of both inner and outer wing parts gives birds the ability to generate a net lift during the alternating flapping cycle. Moreover, the feathers act alongside the movement altering the aerodynamic properties of the wing in favor of the net lift.

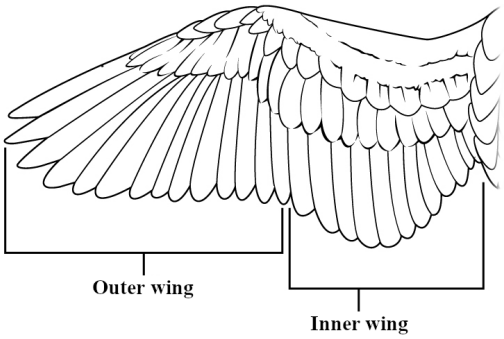

Figure 1. Avian wing structure (adapted from Wikimedia Commons)

In light of natural observations and high-speed photography of bird flight some inspiration and guidelines can be obtained for the ideal trajectory of the wing. Within this article's scope, we can assume both wing parts act as a rigid bar. That way, the inner wing follows a simple arch around the body, while the outer wing rotates about the former, following a combined and more complex trajectory.

The mechanisms described in this paper aim to reproduce the wing movement on the frontal plane, i.e. considering the height and wingspan axes. Therefore, an analysis on Fig. (2) and observations present in Arenas (2016) gives some insight on the desired range of movement for inner and outer wing. The figure shows us four frames composing a full flapping cycle. We can see that the inner wing rotates from it's maximum angle at around 35^o to an horizontal position (0^o). In turn, the outer wing can be analyzed starting from frame 2, where it starts to move down. Between frames 2 and 4, the outer wing ranges from a minimum of 150^o to a maximum of 215^o, then, at frames 4 and 1, rapidly rises to it's starting position (frame 2).

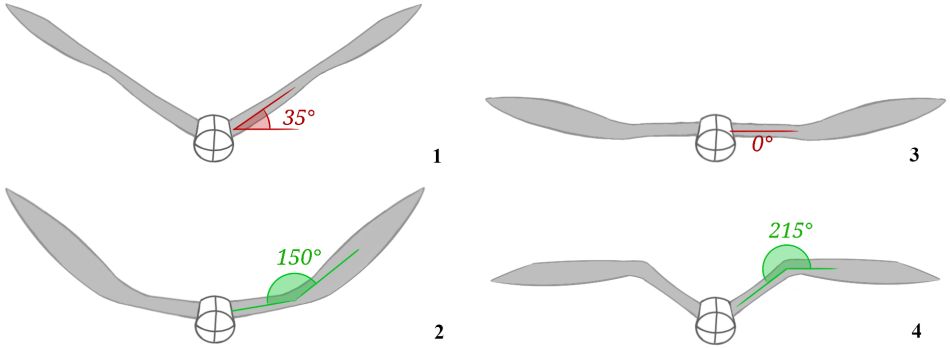

Figure 2. Angular ranges for inner and outer wing, analysis of video at Festo USA (2012) [adapted from Arenas (2016)]

3. MECHANICAL DESIGNS

There are many mechanical designs able to emulate the flapping movement of a bird's wings. Particularly, most of the simpler ones use the four-bar linkage as their main component, which will be the kind of mechanism studied in this paper. These minimal designs, composed of one to three four-bar linkages, can be easy to build and offer great energy efficiency while having a wide range of possible movements and trajectories. Three of those designs can be seen on Fig. (3) below.

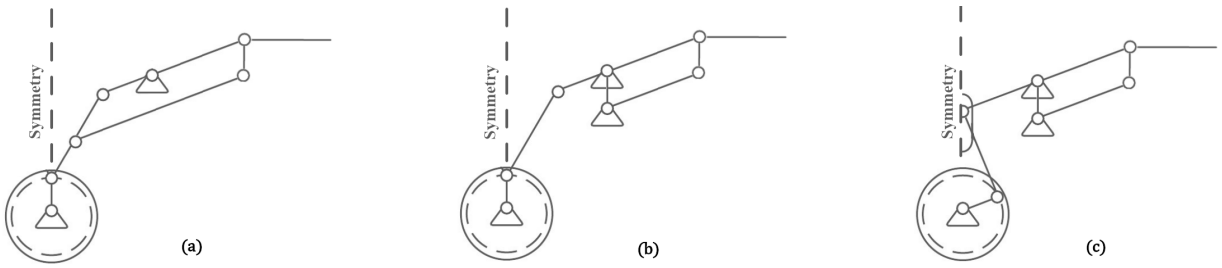

Figure 3. Examples of flapping wing mechanism design. (a) Single-crank double-rocker design, secondary mechanism with coupled frame. (b) Single-crank double-rocker design, secondary mechanism with fixed frame. (c) Single-crank single-rocker sliding design, secondary mechanism with fixed frame.

To reproduce the distinct parts of the wing and their movements, the mechanisms are made of a base four-bar linkage and a secondary coupled mechanism that makes up the outer wing. They differ by two main aspects: a sliding mechanism component and the outer wing coupling. The sliding component in mechanism (c) aims to reach perfect synchrony from both sides. In fact it does, but also adds considerable friction and energy loss to the device.

Considering the coupling aspect, designs (b) and (c) have a secondary mechanism with a fixed bar, where the only coupling between primary and secondary parts is a shared bar. On the other hand, mechanism (a) exhibits an elaborate coupling, where the former "fixed" bar is coupled to the primary mechanism while they also share another bar. That way, the outer wing is able to execute complex trajectories, giving the design room for optimization and fine-tuning.

We can also note that it's possible for some designs to work with double cranks, which ensures synchrony between both sides but adds considerable complexity to the mechanisms. The ones presented above work on a single crank, providing a direct coupling from the driving motor to the mechanism. However, that makes the movement of both sides necessarily different, which leads to the main problem: asynchrony.

Balancing the mechanical simplicity alongside the complexity of movement from the seen designs, the single-crank double-rocker mechanism with fully coupled outer wing (mechanism "a" on Fig. (3)) was chosen as our focus. This design offers a great range of possible movements and trajectories, necessary for the desired optimization, but also maintains mechanical simplicity having a single driving crank.

As noted, a single crank mechanism introduces asynchrony, which needs to be minimized. Particularly, the coupling used in the secondary part of the chosen mechanism is very sensible to asynchrony. A small difference in the primary mechanism state will cause a large divergence in the outer wing. In order to meaningfully analyze the mechanism's synchrony, an adjusted position value for the wingtip will be defined in the following sections.

4. MATHEMATICAL FORMULATION

The first step on mathematically describing the wing mechanism is to name each of its components and variables of interest. The mechanism consists of two four-bar linkages and an additional bar for the outer wing.

Each four-bar linkage has a base bar, also called frame or fixed bar, an input link, called a crank or motor bar, an output link, called a rocker (the third bar) and the fourth bar, called the coupler link. The primary and secondary (inner and outer) mechanisms will have their bars referred to as r_i and s_i, respectively, where i is the bar's index (where index 1 is the base bar, 2 the input link, 3 the output link, 4 the coupler link). For the outer wing additional bar, the letter t will be used. In the expressions that will follow, each variable r_i and s_i, for every index, and t for the outer wing, will represent their corresponding bar lengths.

The connection points between the main links are also identified in the figures and will be important in the analysis of absolute dynamic quantities. They are denoted with capital letters (P for the primary mechanism, Q for the secondary and T for the outer wing), with a sequential index corresponding to one of the links they connect. Some points are shared joining the primary and secondary mechanisms, in those cases, the primary mechanism notation will be preferred.

All linkages and their identification are shown in Fig. (4) where we can see a technical drawing of the mechanism with two representations, one identifying the links and points and other identifying relevant angles. All components and variables of interest depicted will be clarified subsequently.

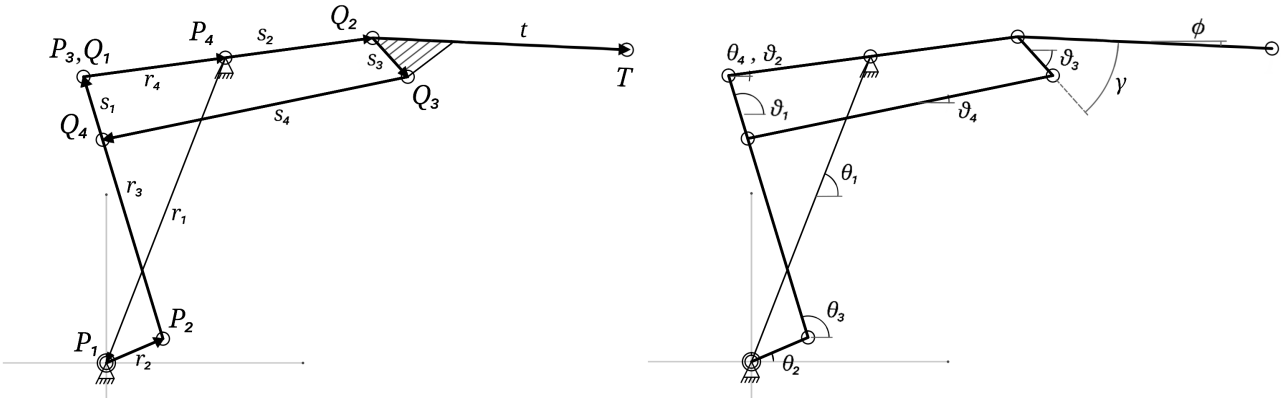

Figure 4. Technical drawing of the flapping mechanism. On the left, connection points and links are identified, showing the two four-bar linkages (P_1-P_2-P_3-P_4 and Q_1-Q_2-Q_3-Q_4). On the right, relevant angles relative to the horizontal are identified.

Besides their lengths, some expressions will represent the bars as vectors, as seen in Fig. (4). The vector names follow from the bars' identifications, using curly brackets to avoid confusion (as in $\{r_i\}$, $\{s_i\}$ and $\{t\}$).

The linkages also have absolute and relative angles associated with each bar. For bar t, i.e. the outer wing, the position angle is ϕ and there is also a constant construction angle γ. Therefore:

$$\phi = \vartheta_3 - \gamma \tag{1}$$

For each bar r_i there is an associated angle θ_i and for secondary bars s_i there are associated angles ϑ_i. It's important to note that the conventional formulation of the four-bar linkage considers the base bar to be fixed and horizontal ($\theta_1 = 0$). To be able to use the conventional expressions, we refer to the relative angles (θ'_2, θ'_3, θ'_4, etc.) defined as below:

$$\theta_i = \theta'_i + \theta_1, \quad i = \{1, 2, 3, 4\} \tag{2}$$

Therefore $\theta'_1 = 0$ and we can apply the mentioned formulation. This change of reference will also be used to describe the secondary mechanism, even though the latter will have a moving reference. We can define the absolute angle ϑ_1 for the secondary mechanism, such as:

$$\vartheta_1 = \theta_3 + \pi \tag{3}$$

And, similarly to Eq. (2):

$$\vartheta_i = \vartheta'_i + \vartheta_1, \quad i = \{1, 2, 3, 4\} \tag{4}$$

Angular velocity and acceleration are also values of interest relating to each link, they are named following the same pattern as the angles and using Newton's notation. As an example, angular acceleration for the secondary mechanism is denoted as $\ddot{\vartheta}_i$. Similarly, the vectors representing relative linear velocity and acceleration at each connection point are the first and second derivatives of the relative position vectors. Absolute values follow the same notation based on the points' names (as in $\{\ddot{P}_3\}$, which is the absolute linear acceleration for point P_3).

With all relevant variables defined, we can start modeling the shape, position and movement of inner and outer wing. As noted, the inner wing design corresponds to a conventional four-bar linkage, which can be described mathematically in terms of the crank relative angle, angular velocity and acceleration (θ'_2, ω_2, α_2). The formulation seen below follows from Norton (2009). However, it's important to note that as the mechanism's simulation and optimization was carried out using Python Programming Language and therefore some expressions differ from the original source in ways that provide performance improvements. The final formulation is the one presented below.

Knowing the crank relative angle θ'_2 we can calculate θ'_3 and θ'_4. As the full expressions are quite complex, it's useful to define some intermediary variables. The formulation follows:

$$\theta'_3 = 2arctg\left(\frac{-E \pm \sqrt{E^2 - 4DF}}{2D}\right) \tag{5}$$

$$\theta'_4 = 2arctg\left(\frac{-B \pm \sqrt{B^2 - 4AC}}{2A}\right) \tag{6}$$

Where the intermediary values (A, B, C, D, E, F) are:

$$A = -K_A + (K_C + 1) \cdot cos\theta_2' + K_D \quad (7) \qquad D = -K_A + (K_B + 1) \cdot cos\theta_2' + K_E \quad (9)$$

$$C = +K_A + (K_C - 1) \cdot cos\theta_2' + K_D \quad (8) \qquad F = +K_A + (K_B - 1) \cdot cos\theta_2' + K_E \quad (10)$$

$$B = E = -2sin\theta_2' \quad (11)$$

And also, (K_A, K_B, K_C, K_D, K_E) are defined as:

$$K_A = \frac{r_1}{r_2} \quad (12) \qquad K_B = \frac{r_1}{r_3} \quad (13) \qquad K_C = \frac{r_1}{r_4} \quad (14)$$

$$K_D = \frac{r_3^2 - r_2^2 - r_4^2 - r_1^2}{2r_2r_4} \quad (15) \qquad K_E = \frac{r_4^2 - r_2^2 - r_3^2 - r_1^2}{2r_2r_3} \quad (16)$$

Knowing θ_1, we now have all essential angles to describe the position of each bar. It is also possible to write all the primary bars as vectors, as shown in Eq. (17).

$$\{r_i\} = r_i \cdot e^{j\theta_i}, \quad i = \{1, 2, 3, 4\} \quad (17)$$

With also known crank angular velocity (ω_2) and acceleration (α_2) the respective values for all other bars in the inner wing can be obtained. For the angular velocity, we have:

$$\omega_3 = \omega_2 \cdot \frac{r_2}{r_3} \cdot \frac{sin(\theta_4 - \theta_2)}{sin(\theta_3 - \theta_4)} \quad (18) \qquad \omega_4 = \omega_2 \cdot \frac{r_2}{r_4} \cdot \frac{sin(\theta_2 - \theta_3)}{sin(\theta_3 - \theta_4)} \quad (19)$$

From that, linear relative velocities can be known for all the connection points.

$$\{\dot{r_i}\} = j \cdot \{r_i\} \cdot \omega_i \quad (20)$$

And following, we can also calculate angular acceleration:

$$\alpha_3 = \frac{\{r_4\} \times K_\alpha}{\{r_3\} \times \{r_4\}} \quad (21) \qquad \alpha_4 = \frac{K_\alpha \times \{r_3\}}{\{r_3\} \times \{r_4\}} \quad (22)$$

Where the intermediary value K_α is used to simplify the expressions, as defined below:

$$K_\alpha = \alpha_2 \cdot \{r_2\} + \sum_i \left[j \cdot \{r_i\} \cdot (\omega_i)^2 \right] \quad (23)$$

Similarly to velocity, we can calculate linear accelerations for the connection points:

$$\{\ddot{r_i}\} = \{r_i\} \cdot (j\alpha_i - \omega_i^2) \quad (24)$$

Now, to model the outer wing, we go back to Fig. (4) to describe the coupling between both mechanisms. As noted at Eq. (3), the frame coupling is $\vartheta_1 = \theta_3 + \pi$ and also, the crank coupling can be written as $\vartheta_2 = \theta_4$. Next, ϑ_2' follows from Eq. (4) and all the expressions written for the inner wing can be used to describe the outer wing (Eq. (12) through (24)). However, as the outer wing frame is not fixed, but rotates along with the primary mechanism, some adjustments have to be done to some equations. The coupling is already accounted for when ϑ_1 is calculated, so all the angular position expressions stay the same. For angular velocity, we can first write:

$$\psi_2 = \omega_4 - \omega_3 \quad (25)$$

As the angular velocities must be relative to the frame, we need to account for it's velocity when describing the input bar coupling. Doing this, the other angular velocity equations are valid the way they were written. The same is true for angular acceleration, therefore $\beta_2 = \alpha_4 - \alpha_3$.

Now for the wingtip, considering Eq. (1), we have:

$$\{T\} = t \cdot e^{j\phi} \quad (26)$$

With all angular dynamic values and relative linear dynamic vectors described, we can develop expressions for absolute linear velocity and acceleration at each connection point. We can write:

$$\{P_1\} = 0 + 0j \quad \text{and} \quad \{P_i\} = \{P_1\} + \sum_{n=2}^{i} \{r_n\}, \quad i = \{2, 3, 4\} \quad (27)$$

With the position vectors determined, obtaining the velocity and acceleration is trivial. The same process can be followed, as the relative vectors for both velocity and acceleration are already determined. Changing or focus to the secondary mechanism, the only necessary adaption is that $\{Q_1\} = \{P_3\}$. Again, the expressions are valid for velocity and acceleration too.

5. OPTIMIZATION AND CODE

With the mechanism design chosen and all necessary dynamic variables fully described, we can focus on the synchrony optimization. As noted on Section (2), the synchrony of the mechanism will be analyzed in respect to the wingtip's position and movement direction. To capture all the desired factors in a simple expression, the formulation below, developed by the author, will be used:

$$Y_r = \text{sgn}(\{\dot{T}\}_y) \cdot \frac{\{T\}_y - \{T\}_{y,min}}{\{T\}_{y,max} - \{T\}_{y,min}} \tag{28}$$

In the expression above, Y_r indicates the adjusted relative position value and $sgn()$ is the sign function. The subscript y indicates the vertical component of the correspondent vector, and the subscripts min and max denote the lowest and highest value, respectively, for that variable reached along the full flapping cycle.

With that value defined, we can now calculate the *asynchrony magnitude* z as the difference between the relative positions of both sides of the mechanism, adjusting for the cyclic nature of the movement:

$$z = 1 - ||Y_{r,right} - Y_{r,left}| - 1| \tag{29}$$

Where $Y_r, right$ and $Y_r, left$ are the relative positions of right and left wings, respectively.

Now, to efficiently optimize the design, all bar sizes and the primary frame angle must be considered as parameters. However, not all combinations of sizes and angles have to and should be considered. Certain mechanisms will have very large synchrony, but they may be unusable for our purposes due to their shape and characteristics. Therefore, in order to limit the parameter space and to restrain the possibilities to desired shapes, relations and ranges were set for some variables. The first applied restraint will be normalization, the primary mechanism's frame will have a fixed length of one and all other link lengths will be relative to this frame. All the restraints can be seen on Tab. (1).

Table 1. Restraints for optimization parameters

Parameter	Minimum value	Maximum value
r_1	1	1
r_2	0.1	0.5
r_3	0.5	1.25
r_4	0.1	0.5
s_1	0.1	0.75
s_2	1.5	1.5
s_3	0.05	0.4
s_4	0.5	1.75
θ_1	0.5 rad	1.25 rad

As the aggregate of all expressions needed to describe the mechanism's asynchrony are quite complex and even with the chosen restraints a parameter space with good precision constitutes billions of possibilities, a fast optimization method is critical. With that in mind, the formulation was implemented and ran in a GPU CUDA environment, which calculates the desired results for many different parameter sets at once. That way, the synchrony of all intended mechanisms can be obtained and compared in a reasonable time.

6. RESULTS

Even with a good optimization parameter, like the value defined in Eq. (29), the "best" mechanism could have some relevant drawbacks not captured by the optimized parameters. Therefore, not only the first, but the ten best mechanisms were returned from the code and compared in order to make our final choice. We can see these mechanisms and their characteristics in Table (2) below.

Table 2. Code output: the ten most synchronous designs

Design	r_1	r_2	r_3	r_4	s_1	s_2	s_3	s_4	θ_1
1	1.0	0.1	0.828125	0.40625	0.1625	1.5	0.3125	1.625	1.226
2	1.0	0.1	0.828125	0.40625	0.1625	1.5	0.356	1.625	1.226
3	1.0	0.1	0.875	0.36	0.1625	1.5	0.356	1.71875	1.226
4	1.0	0.1	0.875	0.40625	0.1	1.5	0.26875	1.71875	1.13
5	1.0	0.1	0.875	0.40625	0.1	1.5	0.356	1.53125	1.226
6	1.0	0.1	0.875	0.40625	0.1625	1.5	0.26875	1.71875	1.13
7	1.0	0.1	0.875	0.40625	0.1625	1.5	0.312	1.625	1.226
8	1.0	0.1	0.875	0.40625	0.1625	1.5	0.356	1.625	1.226
9	1.0	0.1	0.921875	0.31875	0.1	1.5	0.356	1.8125	1.226
10	1.0	0.1	0.921875	0.40625	0.1625	1.5	0.26875	1.625	1.226

Some problematic characteristics that can arise in the generated mechanisms are linkage interference, where both sides of the mechanism go over each other, and undesired trajectories or position. One example of a "bad" design is the first on the table, which has almost perfect synchrony, shown on Fig. (5).

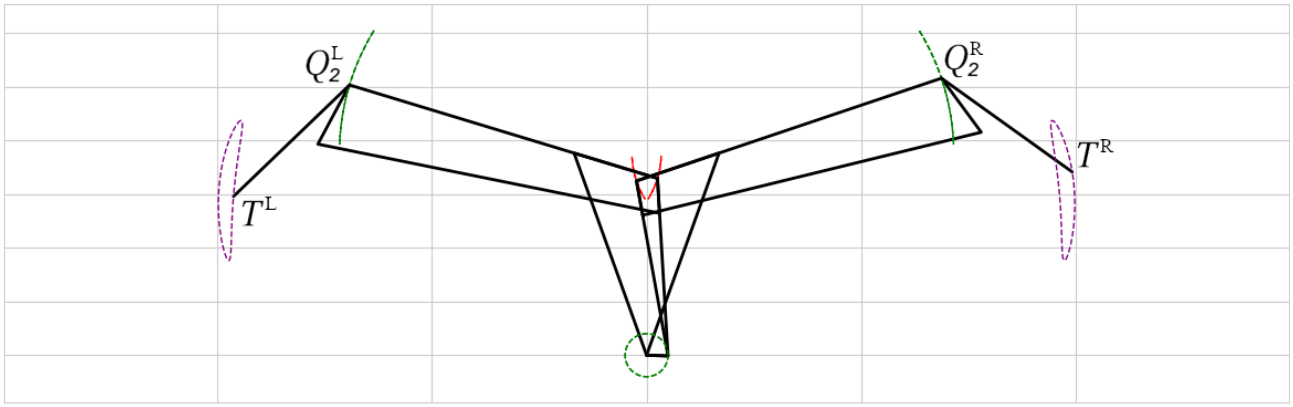

Figure 5. Example of non-ideal mechanism design. At the center the colliding bars can be observed. (Static frame from animation)

After plotting and visualizing all obtained designs, number 9 on Tab. (2) was chosen as having the best overall shape and desirable wing trajectory. The mechanism can be seen on Fig. (6) below.

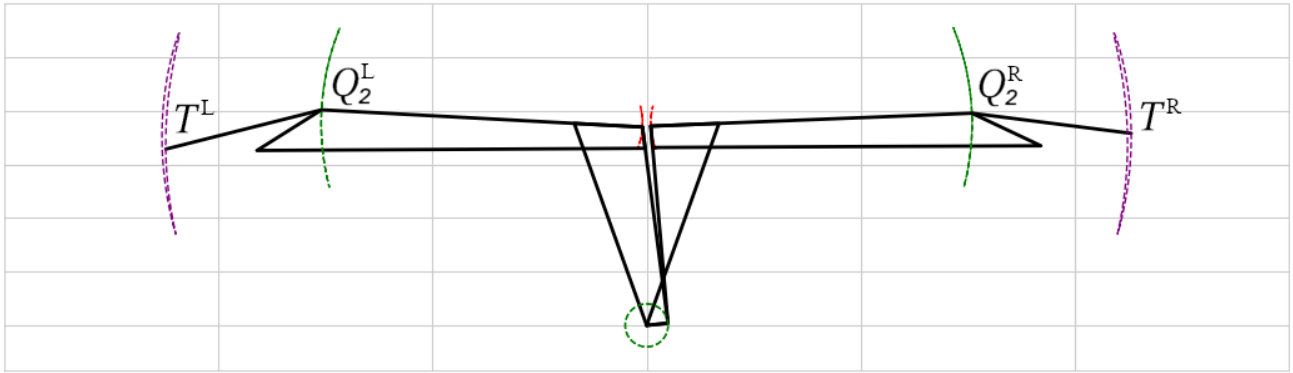

Figure 6. Acceptable mechanism design. The design has adequate proportions and no colliding bars. (Static frame from animation)

6.1 Kinematic analysis

Keeping in mind the practical application of the mechanism it's also essential to assert that not only it has a desirable overall shape and low asynchrony, but also it's kinematic characteristics are adequate. Firstly, as noted on Sec. (2) there are some reference angular ranges for inner and outer wing during the flapping cycle. To allow the correlation with existing research, some new angular values must be defined. All relevant angles are plotted below as functions of the input angle

(θ_2). The values analyzed are Ψ, θ_4, ϕ and λ. Where the transmission angle (Ψ) and relative angle (λ) are:

$$\Psi = \pi + \theta_4 - \theta_3 \tag{30}$$

$$\lambda = \theta_4 - \phi \tag{31}$$

Figure (7) shows us the angles between the rocker arm (r_3) and the inner wing bar (s_2), called transmission angles (Ψ), and between the inner and outer wing (t), called relative angle (λ). Ideally, for maximum torque, the transmission angle should stay close to 90^o with a maximum deviation (called asymmetry angle) of 30^o as concluded experimentally by YANG and Esakki (2021). The limits for the transmission angle can be seen on the graph and are obeyed by the mechanism.

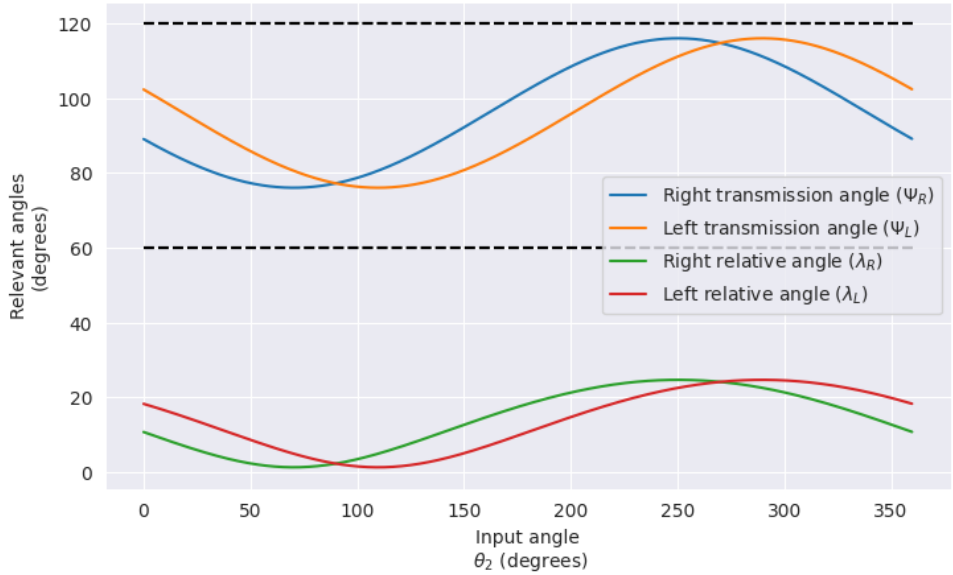

Figure 7. Transmission angles and relative angles for both sides of the wing. The lines in black represent the defined limits for the transmission angles. The subscripts R and L indicate the wing-side the variable corresponds to.

Other relevant angle to be analyzed is the inner wing angle (θ_4), also called oscillation angle. As noted by Arenas (2016) it's important for the oscillation range to stay within a maximum of 40^o. Figure (8) shows us the oscillation angle and outer wing angle (ϕ) for both wing sides. We can verify that the oscillation angle respects the specified boundary.

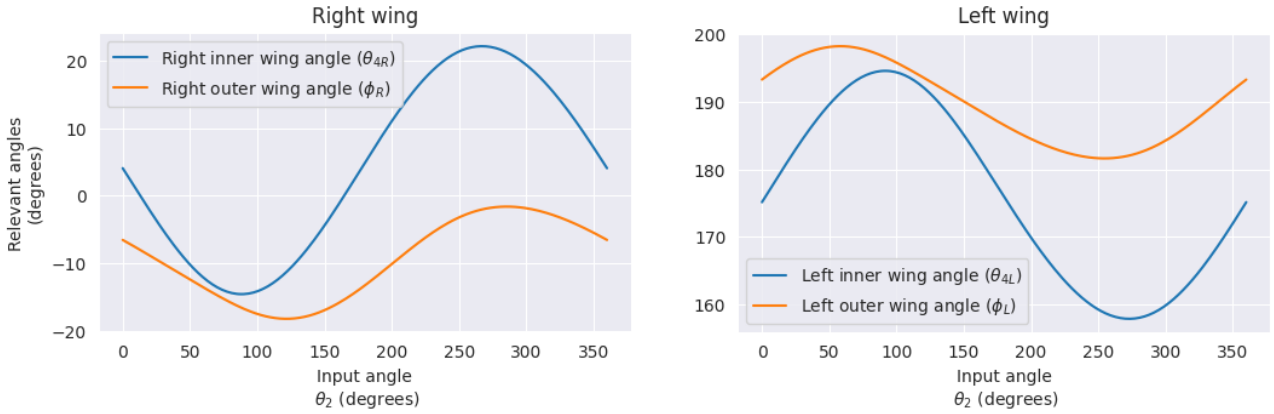

Figure 8. Inner and outer wing angles for both sides. It can be noted that inner wing angles maintain a range within desired limits. The subscripts R and L indicate the wing-side the variable corresponds to.

Now, to analyze dynamic values on the mechanism, particularly in the wingtip, we need to first define a reference scale and flapping rate. Based on observation data for real birds, we can stipulate a base scale of 0.15m (r_1 length) and a maximum rate of 5 cycles per second, corresponding to a medium sized bird. Figure (9) shows the resulting magnitudes for velocity and acceleration at the wingtip (point T).

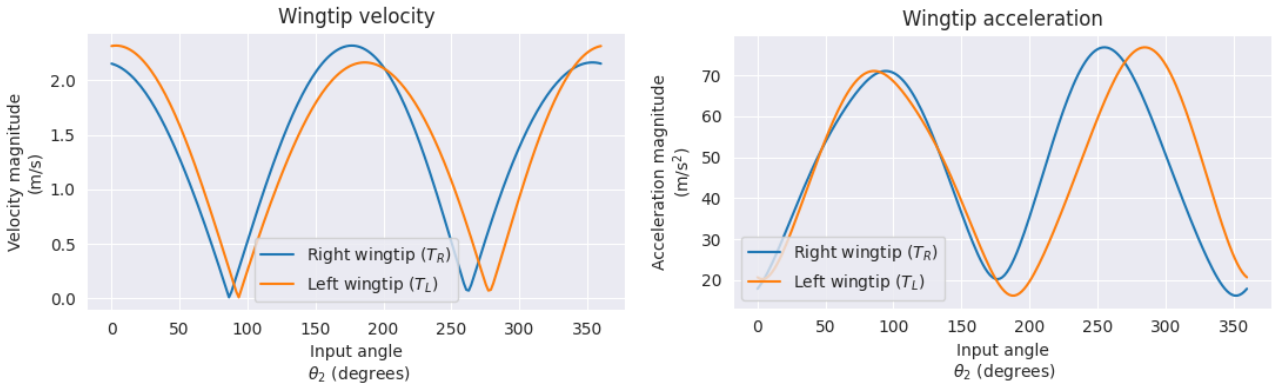

Figure 9. Velocity (left) and acceleration (right) magnitudes for point T (wingtip) on both wing-sides.

Additionally, in order to maintain the stability and mechanical integrity of the mechanism, while also keeping torque on a reasonable level, we will assert that velocity and acceleration at all points stay within practical boundaries. Table (3) wraps-up all relevant maximum values for each point on the mechanism.

Table 3. Maximum dynamic magnitudes for points in the mechanism

Point/Parameter	P_1	P_2	P_3	P_4	Q_1	Q_2	Q_3	Q_4	T
Velocity (m/s)	0.00	0.47	0.48	0.00	0.48	1.78	1.98	0.48	2.32
Acceleration (m/s^2)	0.00	14.80	16.87	0.00	16.87	62.50	67.79	16.62	76.87

6.2 Asynchrony analysis

With the preferred design chosen, we can now focus on analyzing more of it's characteristics. As already noted, it has a maximum asynchrony of 0.081, that is, the two sides deviate by around 8% of their vertical range. But it is also interesting to observe how the synchrony changes along the flapping cycle. A graph plotting asynchrony as a function of the primary input angle (θ_2) can be seen on Fig. (10).

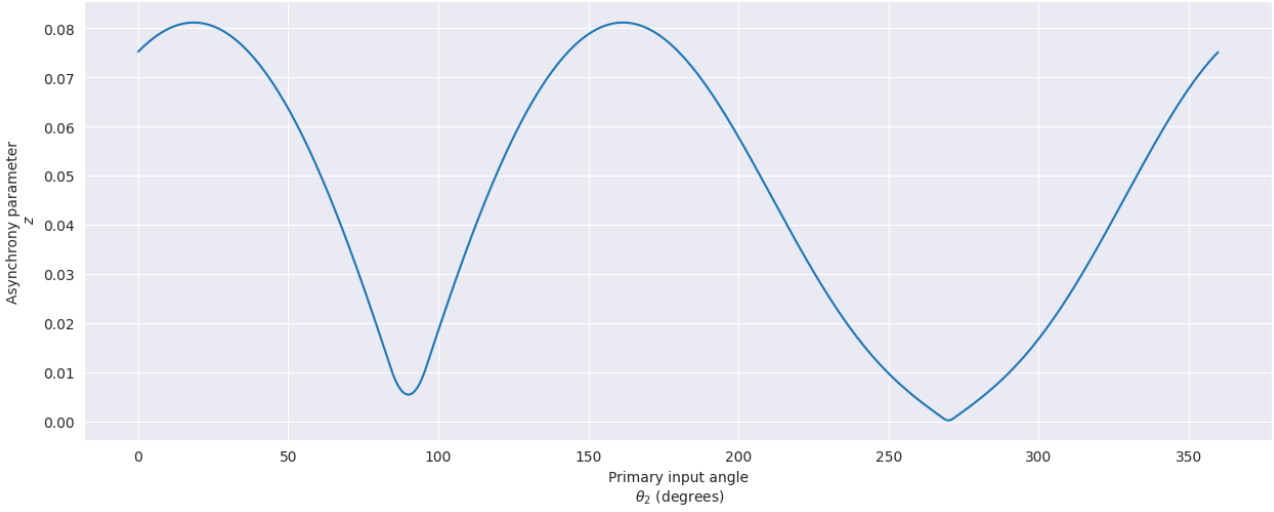

Figure 10. Asynchrony and input angle relation

7. CONCLUSION

With the methods described and the development made in this work we could achieve a desirable design for a flapping-wing mechanism with a single drive and high synchrony, which was our first goal. Further research and fine-tuning on the optimization code and parameters are going to allow even better results, which could then be applied on great and efficient FWAV designs.

Additionally, the analysis developed in this paper was able to shed some light on the effects of each linkage dimension on the overall synchrony of the mechanism. This provides clarity to manually tune the obtained mechanisms in order to

precisely fit one's goals. Furthermore, we could observe that there's a direct and inverse relation of range and complexity of movement with the synchrony of the mechanism. That leads us to conclude that for more precise and advanced applications, requiring fine-tuning and a diversity of possible trajectories, a single drive mechanism is not a great choice.

8. ACKNOWLEDGMENT

The fourth and fifth authors thank the São Paulo Research Foundation (FAPESP), Grant number 22/03128-7.

9. REFERENCES

Alexander, D.E., 2004. *Nature's Flyers: Birds, Insects, and the Biomechanics of Flight*. Johns Hopkins University Press.

Arenas, P.A.L., 2016. *Dynamics of the Herring Gull Wings: An Underactuated Approach*. Master's thesis, Faculty of Engineering, Department of Mechanical Engineering, Bogotá D.C., Colombia.

Festo USA, 2012. "SmartBird - Bird's flight decoded". `festo.com/us/en/e/aboute-festo/research-and-development/bionic`

Norton, R.L., 2009. *Kinematics and Dynamics of Machinery*. McGraw-Hill.

Send, W., Fischer, M., Jebens, K., Mugrauer, R., Nagarathinam, A. and Scharstein, F., 2012. "Artificial hinged-wing bird with active torsion and partially linear kinematics".

Shi, Y., He, W., Guo, M., Xia, D., Luo, X. and Ji, X., 2022. "Mechanism design and motion analysis of a flapping-wing air vehicle".

YANG, L.J. and Esakki, B., 2021. *Flapping Wing Vehicles: Numerical and Experimental Approach*. CRC Press.

10. RESPONSIBILITY NOTICE

The authors are solely responsible for the printed material included in this paper.